Power-to-Fuel Pathway: Sustainable E-Fuel Production Using Green Hydrogen and CO_2 Capture

Bilel Hadrich[a,b]*

[a]Imam Mohammad Ibn Saud Islamic University (IMSIU), Riyadh 11432, Saudi Arabia"
[b]Laboratory of Enzyme Engineering and Microbiology, Engineering National School of Sfax (ENIS), University of Sfax, P.O. Box 1173, Sfax, 3038, Tunisia

* Corresponding author; E-mail: bmhadrich@imamu.edu.sa; ORCID: 0000-0002-0671-4018

Submitted 03/03/2026, Accepted 08/08/2026, Available online 25/09/2026, Published 31/12/2026
DOI: 10.64518/uohjs.2026.05

Abstract:
This study presents the design of an electro-fuel (e-fuel) production process (EFPP) using hydrogen from water and carbon dioxide from atmospheric air. The project aims to produce sufficient e-fuel to supply the annual fuel demand of a community of 10,000 people in Saudi Arabia. EFPP uses a Reverse Water–Gas Shift (RWGS) reactor, a Fischer–Tropsch (FT) reactor, a three-phase separator, heat exchangers, and other supporting equipment to prepare the feedstock and purify the final products. The material and energy balances were developed to simulate process performance using AspenOne Engineering® V14 (2022) software. EFPP requires 12,230 $kg \cdot h^{-1}$ of water to produce green hydrogen by electrolysis, which accounts for about 80% of the total energy demand (67.84 MW). Solar power can supply the required energy for this system. Moreover, EFPP processes 15,620 × 10^3 $kg \cdot h^{-1}$ of air to extract CO_2. The hydrogen reacts with captured CO_2 in the RWGS reactor to produce carbon monoxide (CO) and water. The CO is then fed to the FT reactor, where it reacts with additional hydrogen to synthesize liquid e-fuels (C_5–C_{11}). Technical feasibility was assessed by designing and sizing the main process units, including the RWGS reactor, the FT reactor, the three-phase separator, and the key heat exchanger. EFPP produces liquid e-fuels mainly composed of n-octane (99.9%) at about 1,674 $kg \cdot h^{-1}$, with an estimated production cost of around 1.55–1.76 USD per liter. The results show that renewable-based e-fuel production is technically feasible and economically promising.

Key words: *e-fuel, hydrogen, carbon dioxide, design, renewable resources.*

1. INTRODUCTION

The climate crisis has become an immediate global emergency because human greenhouse gas emissions (GHG) have reached historic levels. The climate crisis creates visible effects which impact the environment, human health, and the global economy according to Pathak *et al.* (2025), Pathak *et al.* (2023), IPCC (2023), and IPCC (2022). Solving this problem requires full decarbonization of the energy sector, as it remains the largest source of GHG emissions.

Developing renewable energy and improving efficiency are important steps, but emerging technologies such as green hydrogen, carbon capture, and synthetic e-fuels offer effective solutions for a cleaner and more sustainable energy system through the Power-to-Liquid (PtL) pathway.

The system studied in this work is an e-fuel production process (EFPP). It begins with hydrogen production through water electrolysis using renewable electricity, enabling a low-carbon process. The Reverse Water Gas Shift (RWGS) reaction converts CO_2 captured from air into CO, producing a syngas stream with a suitable H_2/CO ratio for further synthesis. In a Fischer–Tropsch (FT) reactor, the

conditioned syngas is converted into long-chain hydrocarbons, which are then processed into drop-in fuels such as e-kerosene, e-diesel and e-gasoline (Farhani *et al.*, 2025; Pathak *et al.*, 2025; Bube *et al.*, 2024; Choi *et al.*, 2024; Farhani *et al.*, 2024; Pathak *et al.*, 2023).

A major advantage of e-fuels is their compatibility with existing fuel-distribution infrastructure and combustion engines. Moreover, the CO_2 emissions from fuel combustion can achieve theoretical balance with CO_2 emissions that are captured during the extraction process, which creates a closed carbon cycle system.

PtL system performance depends on key operating factors such as electrolysis efficiency, RWGS conversion, FT selectivity, heat integration, and overall energy efficiency. Early studies suggest that fossil fuel particulate emissions can be reduced, but full life-cycle assessments are still needed to evaluate environmental impacts and support large-scale deployment. Therefore, rigorous process simulation, optimization, and techno-economic analysis are essential to determine whether renewable PtL systems are both environmentally and economically viable in low-carbon energy infrastructures (Farhani *et al.*, 2025; Pathak *et al.*, 2025; Bube *et al.*, 2024; Choi *et al.*, 2024; Farhani *et al.*, 2024; Pathak *et al.*, 2023).

This study evaluates a renewable e-fuel production system that could meet the annual energy demand of a community of 10,000 people in Saudi Arabia. The process combines Direct Air Capture of CO_2 with green hydrogen production by renewable-powered electrolysis, forming a closed carbon cycle. It also supports Saudi Vision 2030 by promoting energy transition, improving energy security, and encouraging sustainable economic growth.

2. DESIGN AND MODELLING

2.1. Plant design, modelling and simulation

AspenOne Engineering® Version 14 (2022) is widely regarded as a leading and robust software platform for industrial process simulation. In this study, AspenOne Engineering® V14 (2022) was employed to design, model, and simulate the entire system, enabling the calculation of comprehensive material and energy balances at both the overall process level and for individual unit operations.

The Peng–Robinson model was used to determine the thermodynamic properties of all components.

2.2. Process of CO_2 capture and storage from air

Direct Air Capture (DAC) technology, studied in several research articles (Chauvy and Dubois, 2022a, 2022b; Keith *et al.*, 2018 Sanz-Pérez *et al.*, 2016) shows strong potential as an eco-friendly method for removing carbon dioxide. DAC systems use different methods for separation which include physical absorption, chemical absorption, adsorption, and membrane separation.

The amine-based chemical absorption method was selected for this study due to its high selectivity and efficiency.

Amines are organic nitrogen compounds with various chemical forms. Methyl diethanolamine (MDEA, $CH_3N(C_2H_4OH)_2$) is a tertiary amine solvent used industrially, valued for its CO_2 loading capacity of 1.0 mole per mole of amine—higher than that of other common amines (Chauvy and Dubois, 2022a, 2022b; Ivanov *et al.*, 2017, Sanz-Pérez *et al.*, 2016; Santos *et al.*, 2014; Yu *et al.*, 2012). The main absorption process is shown in Eq. (1) (Kierzkowska-Pawlak and Chacuk, 2010; Versteeg, and Swaaij, 1988):

$$MDEA + H_2O + CO_2 \longrightarrow MDEAH^+ + HCO_3^- \quad (1)$$

This process uses two main columns: an absorber and a stripper (regenerator). Ambient air containing CO_2 enters the bottom of the absorber, where the solvent absorbs the CO_2, forming a CO_2-rich amine solution. This rich solvent moves to the stripper for thermal regeneration. Heating the solvent to high temperatures releases CO_2, while the regenerated amine returns to the absorber. The desorbed CO_2— now high purity and under elevated pressure—can be transported for utilization or storage.

The absorber operates at about 101.3 kPa and 40–60 °C, while the stripper operates at 120–140 °C (Sanz-Pérez *et al.*, 2016; Yu *et al.*, 2012).

In this work, the DAC unit was modeled using a simplified approach in AspenOne Engineering®, where CO_2 separation was represented as a stripping operation. A rigorous simulation of the full DAC process—including air contactor design, absorption at very low CO_2 concentrations, and solvent regeneration—is still challenging within the current AspenOne Engineering framework.

As a result, the regeneration heat duty and part of the auxiliary energy demand (e.g., fan/blower work) were not explicitly included. This simplification may underestimate the total energy requirement and lead to an optimistic evaluation of process efficiency.

According to the literature, DAC systems require significant thermal and electrical energy, with regeneration heat duties of 3.5–8 MJ per kg of CO_2 and electricity consumption of 0.72–1.8 MJ per kg of CO_2 (Keith *et al.*, 2018; Sanz-Pérez *et al.*, 2016; Chauvy and Dubois, 2022a, 2022b).

2.3. H_2 production *via* water electrolysis

Hydrogen can be produced by several methods, including water electrolysis, stream methane reforming, and biomass gasification. Among these, water electrolysis—especially when powered by renewable energy sources such as solar or wind—offers key advantages, including high hydrogen purity, lower environmental impact, and zero greenhouse gas emissions.

In this study, water electrolysis was selected due to its technical and environmental benefits. The process uses an electrochemical system to split water into hydrogen and oxygen through redox reactions occurring in an electrochemical cell (Eq. 2).

$$H_2O \longrightarrow H_2 + \frac{1}{2}O_2 \tag{2}$$

Hydrogen is produced at the cathode and oxygen at the anode when an external voltage exceeding the thermodynamic threshold is applied. The production rate depends on the current, following Faraday's law. Charge balance is maintained by ion transport through the electrolyte (Farhani *et al.*, 2025; Pathak *et al.*, 2025; Bube *et al.*, 2024; Choi *et al.*, 2024; Farhani *et al.*, 2024; Pathak *et al.*, 2023).

The electrolyzer was modeled in AspenOne Engineering® as a conversion reactor using Eq. 2, assuming 100% efficiency for simplicity.

2.4. CO production *via* reverse water-gas shift reactor

The captured CO_2 from DAC and the H_2 from the electrolyzer both enter the Reverse Water Gas Shift (RWGS) reactor. The reactor uses catalytic hydrogenation reactions to transform the gases into carbon monoxide (CO), as described in Eq. (3).

$$CO_2 + H_2 \longrightarrow\!\!\!\!\!\!\leftarrow\ CO + H_2O \tag{3}$$

The RWGS reaction needs high temperatures (about 600–800 °C) because it absorbs heat. Catalysts such as copper, iron, nickel, or molybdenum carbide are used to improve efficiency and increase CO production.

The RWGS reaction produces the desired product, but at lower temperatures and near-atmospheric pressures, unwanted side reactions can occur and interfere with the main process. These side reactions form methane, which reduces the efficiency of carbon monoxide production (Torres-Sempere *et al.*, 2025).

One major side reaction is the direct hydrogenation of CO_2 to methane (CO_2 methanation) (Eq. 4).

$$CO_2 + 4\ H_2 \longrightarrow CH_4 + 2\ H_2O \tag{4}$$

Another side reaction is the hydrogenation of CO to methane (CO methanation) (Eq. 5).

$$CO + 3\ H_2 \longrightarrow CH_4 + H_2O \tag{5}$$

Both reactions are exothermic, with standard reaction enthalpies of $\Delta H_4^\circ = -165\ kJ/mol$ and $\Delta H_5^\circ = -206\ kJ/mol$, respectively.

Therefore, careful control of temperature, pressure, and catalyst is essential to maximize CO production and reduce methane formation. In this work, the RWGS reactor was modeled in AspenOne Engineering® as a conversion reactor using Eq. (3), neglecting side reactions due to the high pressure

(~2000 kPa). An efficiency of 39.91% was assumed using a Cu/ZnO catalyst (Phey *et al.*, 2023; González-Castaño *et al.*, 2021).

2.5. E-Fuel production *via* a Fischer–Tropsch reactor

In the Fischer-Tropsch (FT) reactor, CO from the RWGS reaction and hydrogen from electrolysis are combined to form hydrocarbons. FT converts syngas (CO and H_2) into various paraffinic compounds (Eq. 6) (Bube *et al.*, 2024; Choi *et al.*, 2024).

$$n\ CO + (2n+1)\ H_2 \longrightarrow C_nH_{2n+2} + n\ H_2O \quad (6)$$

The exothermic reactions have a standard enthalpy change of $\Delta H_6^{\circ} = n \cdot (-150)\ kJ/mol$.

The e-fuel production cycle ends here, as it produces synthetic hydrocarbons that can be used in existing fuel infrastructure to support carbon -neutral energy systems.

In this study, a production rate of approximately 15 kmol/h of liquid hydrocarbons (C_5–C_{11}, gasoline range) was used as the design basis. This was estimated from Saudi Arabia's per capita gasoline consumption and scaled to a population of 10,000 people (Alwosheel and Dua 2023; Website 1).

Under normal conditions (H_2/CO_2 = 3:1, 320 °C and 2000 kPa), the system achieves about 37% CO_2 conversion. The product distribution shows approximately 8% methane (CH_4), 18% C_2–C_4 hydrocarbons fuel gas, mainly light olefins), 73% C_5–C_{11} hydrocarbons (naphta, liquid fuel), and 1% for C_{12}^+ (diesel) according to Hassan *et al.* (2025), Wei *et al.* (2017), and Daza and Kuhn (2016) (Table 1).

Considering the complexity of the Fischer–Tropsch process, which involves many parallel reactions, only a limited number of representative reactions were selected for this work (Eqs. (7)-(10)). These reactions were used as illustrative cases and modeled in a conversion reactor using AspenOne Engineering® (Table 1), with each reaction corresponding to a typical hydrocarbon in the product distribution.

Table 1. Modeling of Fischer–Tropsch Reactions Using AspenOne Engineering®

Hydocarbon range*	**Distribution (%)**	**Reaction**	**Eq.**
CH_4^g	8	$CO + 3\ H_2 \longrightarrow CH_4 + H_2O$	(7)
C_2–C_4^g	18	$2\ CO + 5\ H_2 \longrightarrow C_2H_6 + 2\ H_2O$	(8)
C_5–C_{11}^l	73	$5\ CO + 11\ H_2 \longrightarrow C_5H_{12} + 5\ H_2O$	(9)
C_{12}^{+l}	1	$12\ CO + 25\ H_2 \longrightarrow C_{12}H_{26} + 12\ H_2O$	(10)
Total	100		

*g: gas; l: liquid

2.6. Complementary process equipment

The EFPP requires additional equipment to handle different temperatures and pressures. To control heat, pressure, and flow , several key units are used.

These include heat exchangers, compressors, mixers, splitters, and separation units such as membrane and gas–liquid separators.

2.7. Unit sizing

The equipment sizing was carried out based on the process design and simulation results. For this stage, several references addressing this type of analysis were consulted (Turton *et al.*, 2012; Towler and Sinnott, 2008; Sinnott, 2005; Peters *et al.*, 2003).

2.7.1 Reverse water gas shift and Fischer–Tropsch reactors

A reactor is a specifically designed vessel in which a chemical reaction occurs under specific conditions. Reactor design is based on the analysis of reaction kinetics, heat and mass transfer, and fluid

flow. The main objectives of reactor design are process optimization, maximum reactant conversion, and ensuring safe, efficient, and reliable reactor operation.

2.7.1.1 Type, catalyst, dimensions and configuration

The reverse water–gas shift (RWGS) and Fischer–Tropsch (FT) reactors were selected as three-phase slurry reactors, comprising gas, solid catalyst, and liquid components. As previously mentioned, the RWGS reactor utilized a Cu/ZnO catalyst, selected to maximize the CO yield at 39.91%, while the FT reactor employed a Co/SiO_2 catalyst, chosen to favor the production of liquid fuels (C_5–C_{11}) compared to other e-fuels (Li *et al.*, 2025; Hassan *et al.*, 2025; Phey *et al.*, 2023).

The RWGS reactor was operated at 750 °C and 2 MPa, while the FT reactor operated at 350 °C and 2 MPa. The selected residence times were based on operating conditions and reactor design considerations reported in previous studies on slurry-phase systems. A residence time of 4 h was selected for the RWGS reactor to ensure sufficient CO formation under the selected operating conditions, whereas a residence time of 36 h was adopted for the FT reactor to account for the slower chain-growth kinetics and product accumulation behavior associated with liquid hydrocarbon (C_5–C_{11}) formation in slurry-phase systems (Hassan *et al.*, 2025; Li *et al.*, 2025; Phey *et al.*, 2023; Masuku *et al.*, 2012; Fox *et al.*, 1991).

The required reactor volume was calculated using Eq. (11):

$$V = \dot{V} \cdot t_R \tag{11}$$

where V is the reactor volume (m^3); $\dot{V}$ is the feed volumetric flow rate ($m^3 \cdot h^{-1}$) obtained from AspenOne Engineering® Version 14 simulations, and t_R is the residence time of the reactants.

If the required volume exceeds 38 m^3, a vertical vessel supported on concrete pads should be used. Accordingly, the height (h) and diameter (d) of the vertical cylindrical vessel were calculated using the optimum height-to-diameter ratio of 3, as recommended by Turton *et al.* (2012) and Peters *et al.* (2003).

Eq. (12) provides the relationship between the reactor diameter and volume.

$$d = \sqrt[3]{\frac{4 \cdot V}{3 \cdot \pi}} \tag{12}$$

2.7.1.2 Impeller

Based on the dynamic viscosity of the reactor mixture, estimated using AspenOne Engineering® V14 simulations, and the calculated reactor volume, a suitable impeller type was selected from standard industrial configurations according to Figures S1 and S2 (Supplementary Data) (Towler and Sinnott, 2008).

2.7.1.3 Mixing power

Based on Table S1 (Supplementary Data), the required mixing power rate (kW/m^3) was determined for the slurry suspension case. After that the mixing power (kW) was determined for both reactors using Eq. (13).

$$Mixing\ Power = V \cdot Mixing\ Power\ rate \tag{13}$$

2.7.1.4 Material of construction

The construction material of the reactors under study was selected according to its compatibility with the operating environment, considering potential interactions between the process mixture and the reactor walls.

2.7.1.5 Vessel thickness

The vessel thickness of the reactors were determined using Eq. (14) (Towler and Sinnott, 2008; Turton *et al.*, 2012).

$$t = \frac{P_{design} \cdot D}{2 \cdot S \cdot E - 1.2 \cdot P_{design}} + CA \tag{14}$$

where t is the vessel wall thickness (m); P_{design} is the design pressure (Pa), taken as $1.1 \cdot P_{max}$ when not otherwise specified; P_{max} is the maximum internal pressure (2 MPa); D is the vessel internal diameter

of the vessel (m); S is the maximum allowable stress of the construction material, obtained from Table S2 (Supplementary Data); E is the weld joint efficiency, which generally ranges between 0.8 and 1 and was assumed to be 0.9 in this study; and CA is the corrosion allowance, taken as 3.8 mm for non-corrosive service.

2.7.1.6 Head and closure

For vessels operating at pressures greater than 1500 kPa, the use of ellipsoidal heads and closures is recommended to ensure mechanical integrity (Sinnott, 2005).

2.7.1.7 Thermal insulation

The reactors are expected to operate at temperatures of 350 °C or higher; therefore, thermal insulation is required to ensure safe operation and to limit heat losses. The insulation system was designed in accordance with the methodology proposed by Turton *et al.* (2012).

2.7.1.8 Heating system

Because the RWGS reaction is endothermic, a continuous supply of superheated steam is necessary to provide the required heat duty. In contrast, the exothermic FT reaction requires continuous cooling water circulation to remove the generated heat. For both reactors, a jacket spacing of 150 mm was adopted, consistent with the recommended range of 50–300 mm (Sinnott, 2005).

2.7.2 Heat exchangers

Heat exchangers are devices designed to transfer heat between two fluids at different temperatures and are extensively used in industries for heating, cooling, and heat recovery applications. Their design requires careful consideration of factors such as heat transfer coefficients, pressure drop, material selection, and thermal efficiency. Common types of heat exchangers include shell-and-tube, plate, and finned-tube configurations. The sizing of these units was performed following the TEMA AEL standards described by Sinnott (2005).

2.7.2.1 Heat rate

After the plant design and simulation steps, each heat exchanger is characterized by its specific heat duty, also called the heat rate (Q in W) transferred between the hot and cold fluids. This heat rate is expressed by Eq. (15).

$$Q = U \cdot A \cdot F_t \cdot LMTD \tag{15}$$

where U is the overall heat transfer coefficient (W/m^2 · K), which was assumed to be $250\ W/m^2 \cdot K$. A is the heat transfer area (m^2). $LMTD$ is the logarithmic mean temperature difference (K), determined using Eq. (16).

$$LMTD = \frac{\left(T_{h_{in}} - T_{c_{out}}\right) - \left(T_{h_{out}} - T_{c_{in}}\right)}{ln\left(\frac{T_{h_{in}} - T_{c_{out}}}{T_{h_{out}} - T_{c_{in}}}\right)} \tag{16}$$

where $T_{h_{in}}$ and $T_{h_{out}}$ are the inlet and outlet temperatures of the hot fluid (K), respectively, and $T_{c_{in}}$ and $T_{c_{out}}$ are the inlet and outlet temperatures of the cold fluid (K), respectively.

$LMTD$ requires a correction factor, F_t, which was calculated using Eq. (17) to account for the heat exchanger configuration and the number of passes. A single pass was selected for both the shell side and the tube side.

$$F_t = \frac{\sqrt{R^2+1} \cdot ln\left(\frac{1-S}{1-R \cdot S}\right)}{(R-1) \cdot ln\left(\frac{2-S \cdot \left(R+1-\sqrt{R^2+1}\right)}{2-S \cdot \left(R+1+\sqrt{R^2+1}\right)}\right)} \tag{17}$$

where R is equal to the shell-side fluid flow rate multiplied by the mean specific heat, divided by the tube-side fluid flow rate multiplied by the tube-side fluid specific heat (Eq. 18) and S is a measure of the temperature efficiency of the heat exchanger (Eq. 19).

$$R = \frac{T_{h_{in}} - T_{h_{out}}}{T_{c_{out}} - T_{c_{in}}} \tag{18}$$

$$S = \frac{T_{c_{out}} - T_{c_{in}}}{T_{h_{in}} - T_{c_{in}}} \tag{19}$$

2.7.2.2 Type

All the heat exchangers were chosen to operate in a countercurrent configuration, and their type is a shell-and-tube heat exchanger.

2.7.2.3 Tube dimensions and configuration

As the first step, the outside diameter (d_o) was selected to provide a suitable heat transfer area while maintaining a reasonable shell diameter. The tube thickness was also selected, to withstand the pressure of the input streams. The inner diameter (d_i) was then calculated accordingly. The tube length was selected based on available standard dimensions.

Subsequently, Eq. (20) was used to determine the number of tubes (N_{tubes}):

$$N_{tubes} = \frac{A}{\pi \cdot d_o \cdot L} \tag{20}$$

Afterward, a square tube arrangement was selected, as it results in a lower pressure drop and provides favorable heat transfer performance. The tube pitch (center-to-center distance between two successive tubes) was calculated as $1.25 \cdot d_o$.

The bundle diameter (D_b) was calculated from equation (21):

$$D_b = d_o \cdot \left(\frac{N_{tubes}}{K_1} \right)^{\frac{1}{n_1}} \tag{21}$$

where K_1 and n_1 are constants obtained from Table S3 (Supplementary data).

The overall diameter of the shell (D_{shell}) was calculated using Eq. (22):

$$D_{shell} = D_b + clearance \tag{22}$$

The $clearance$ term of Eq. (22) represents the shell–bundle clearance, obtained from Figure S3 (Supplementary data) as a function of the selected heat exchanger type and the previously calculated bundle diameter (D_b).

The baffle spacing (B_s) was calculated as $0.4 \cdot D_{shell}$. The baffle cut was chosen to be 25%, as this provides good heat transfer performance while minimizing pressure drop.

2.7.2.4 Overall Heat Transfer Coefficient Verification

Once the heat exchanger dimensions and properties are determined, the design is verified by calculating the overall heat transfer and comparing it with the assumed value.

2.7.3 Three-phase separator

Three-phase separators are widely used in oil and gas production plants to separate oil, gas, and water phases. The design of this equipment involves several considerations, including fluid properties, flow rates, separation efficiency, and vessel dimensions. The main objective is to achieve effective phase separation while maintaining a low pressure drop across the system.

Different separator configurations, including horizontal and vertical designs, present distinct considerations depending on the process requirements. For three-phase separation, a horizontal cylindrical vessel is generally recommended (Sinnott, 2005). The design methodology, equations, and data employed in this work are based on Sinnott (2005).

2.7.3.1 Type, dimensions and configuration

The terminal velocity of the liquid droplets was estimated using Eq. (23):

$$u_t = 0.07 \cdot \sqrt{\frac{\rho_l - \rho_v}{\rho_v}} \tag{23}$$

where ρ_l and ρ_v are the liquid and vapor densities (kg/m^3), respectively.

When a demister pad is used, the settling velocity (u_s) is defined as $0.15 \cdot u_t$. The diameter of the separator (D_v) was determined from the inlet gas flow rate ($\dot{V}_{gases}$) using Eq. (24):

$$D_v = \sqrt{\frac{4 \cdot \dot{V}_{gases}}{\pi \cdot u_s}} \tag{24}$$

Moreover, for pressures up to 2000 kPa, the length-to-diameter ratio is taken as 3, i.e., $L_v = 3 \cdot D_v$. The weir has a specific height (h_l) that regulates the liquid hold-up volume (accumulation) within the separator. It was calculated using Eq. (25).

$$h_l = 0.5 \cdot D_v \tag{25}$$

2.7.3.2 Material of construction

The material of construction was selected as carbon steel due to the non-corrosive environment.

2.7.3.3 Vessel thickness

The vessel thickness was calculated using Eq. (14) where $P_{design} = 1.1 \cdot P_{max}$ ($P_{max} = 110.3\ kPa$); $E = 0.9$ as it generally ranges between 0.8 and 1; $CA = 3.8\ mm$; and $S = 129\ MPa$, which was taken from Table S2 (Supplementary Data).

2.7.3.4 Head and closure

A torispherical head and closure were used, as the pressure was less than 1500 kPa.

3. ECONOMIC ASSESSMENT METHODOLOGY

A preliminary techno-economic analysis (TEA) was performed to evaluate the economic feasibility of the proposed e-fuel production plant (EFPP). The methodology follows established approaches commonly used for chemical process design and economic evaluation (Peters *et al.*, 2003; Towler and Sinnott, 2008; Turton *et al.*, 2012; Chauvy and Dubois, 2022b). The economic assessment considered both capital expenditure (CAPEX) and operating expenditure (OPEX) associated with the major process units, including the electrolyzer, direct air capture (DAC) system, Reverse Water–Gas Shift (RWGS) reactor, Fischer–Tropsch (FT) reactor, compressors, heat exchangers, and separation units.

3.1. Capital expenditure (CAPEX)

The purchased cost of process equipment was estimated using the six-tenths scaling approach (Eq. 26) widely adopted in chemical process design (Peters *et al.*, 2003; Turton *et al.*, 2012):

$$C_2 = C_1 \cdot \left(\frac{S_2}{S_1}\right)^n \tag{26}$$

where C_2 is the estimated equipment cost (USD), C_1 is the reference equipment cost (USD), S_2 and S_1 are the actual and reference equipment capacities, respectively, and n is the scaling exponent, assumed to be 0.6.

The total capital investment of the plant was calculated from Eq. (27):

$$CAPEX = \sum C_{equipment} \cdot FBM \tag{27}$$

where $C_{equipment}$ represents the purchased equipment cost and FBM denotes the bare-module factor.

3.2. Operating expenditure (OPEX)

The annual operating cost, which includes electricity consumption, DAC operation, catalyst replacement, maintenance, and utility costs was calculated using Eq. (28):

$$OPEX = C_{elec} + C_{DAC} + C_{cat} + C_{maint} + C_{util} \tag{28}$$

The annual electricity cost was estimated as (Eq. 29):

$$C_{elec} = P_{elec} \cdot t_{op} \cdot C_{elec,unit} \tag{29}$$

where P_{elec} is the total electrical power requirement (kW), t_{op} is the annual operating time (h/year), and $C_{elec,unit}$ is the electricity price (USD/kWh).

The annual operating time was estimated using Eq. (30):

$$t_{op} = CF \cdot 8760 \tag{30}$$

where CF is the plant capacity factor, assumed to be 90% in this work.

The DAC operating cost was estimated as (Eq. 31):

$$C_{DAC} = \dot{m}_{CO_2} \cdot C_{DAC,unit} \tag{31}$$

where $\dot{m}_{CO_2}$ is the annual CO_2 capture amount (t/year), and $C_{DAC,unit}$ is the DAC cost per tonne of captured CO_2.

3.3. Annualized capital cost and financing assumptions

The capital recovery factor (CRF, Eq. 32) was employed to annualize the total capital cost according to standard process economics procedures (Towler and Sinnott, 2008):

$$CRF = \frac{i \cdot (1+i)^n}{(1+i)^n - 1} \tag{32}$$

The annualized $CAPEX$ was then calculated as (Eq. 33):

$$Annualized\ CAPEX = CAPEX \cdot CRF \tag{33}$$

where i is the discount rate (assumed to be 8%) and n is the plant lifetime (assumed to be 20 years).

The total annualized cost (TAC) was obtained from Eq. (34):

$$TAC = Annualized\ \ CAPEX + OPEX \tag{34}$$

3.4. Economic assumptions

The principal economic assumptions adopted in this study are summarized in Table 2.

Table 2. Economic assumptions used in the economic analysis.

Parameter	Value	Reference
Electricity price	0.04–0.06 USD/kWh	Farhani *et al.* (2024); SERA (2026)
DAC cost basis	246–297 USD/t_{CO2}	Dieterich *et al.* (2020); Chauvy and Dubois (2022b)
Plant capacity factor	90%	Bube *et al.* (2024)
Plant lifetime	20 years	Peters *et al.* (2003)
Discount rate	8%	Towler and Sinnott (2008)
RWGS catalyst lifetime	3 years	González-Castaño *et al.* (2021)
FT catalyst lifetime	3–5 years	Wei *et al.* (2017)
Annual maintenance cost	3–5% CAPEX	Turton *et al.* (2012)

3.5. Sensitivity analysis

A one-factor sensitivity analysis was conducted to evaluate the influence of major economic parameters on the process economics. Electricity price, DAC cost, and plant capacity factor were varied

by ±30% relative to the baseline values. These parameters were selected because they have been identified as key contributors to the economics of Power-to-Liquid systems (Dieterich *et al.*, 2020; Chauvy and Dubois, 2022b; Bube *et al.*, 2024).

3.6. Levelized cost of e-fuel production

The levelized cost of e-fuel (LCOF) was estimated to determine the unit production cost of the generated fuel (Eq. 35):

$$LCOF = \frac{TAC}{\dot{m}_{fuel} \cdot \frac{t_{op}}{\rho_{fuel}}} \tag{35}$$

where LCOF is the levelized cost of e-fuel production (USD/L), TAC is the total annualized cost (USD/year), $\dot{m}_{fuel}$ is the e-fuel production rate ($kg \cdot h^{-1}$), and ρ_{fuel} is the density of the produced fuel ($kg \cdot m^{-3}$).

The LCOF allows comparison between the proposed process and conventional fuels as well as previously reported Power-to-Liquid pathways (Dieterich *et al.*, 2020; Bube *et al.*, 2024).

4. RESULTS AND DISCUSSION

4.1. Plant design

Figure 1 presents the designed plant developed using AspenOne Engineering® Version 14 software.

The system design includes two upstream feedstock generation units that supply feed streams to two catalytic reactors for e-fuel production.

The first feedstock generation unit employs an amine-based chemical absorption system through direct air capture (DAC) technology to capture carbon dioxide (stream #CO2, Figure 1 and Table 3) from ambient air (stream #Air) under atmospheric conditions. The captured and concentrated CO_2 stream (stream #CO2) is subsequently used as the carbon feedstock for downstream processes (Figure 1).

The second unit generates hydrogen through water electrolysis. The electrolyzer, supplied with water, operates at atmospheric pressure and 80 °C and is coupled with a membrane separation unit that produces high-purity hydrogen (stream #H2) and oxygen (stream #O2), with an H_2/O_2 molar ratio of 2 under identical operating conditions (Figure 1 and Table 3). The produced hydrogen can be considered as green hydrogen because it is generated using renewable electricity and produces no direct emissions during the production process . Green hydrogen is considered a key technology for enabling deep decarbonization across various industrial sectors (Farhani *et al.*, 2025; Pathak *et al.*, 2025; Bube *et al.*, 2024; Choi *et al.*, 2024; Farhani *et al.*, 2024; Pathak *et al.*, 2023).

The generated hydrogen stream (stream #H2) is split using TEE-100 and directed to the Reverse Water–Gas Shift reactor (RWGSR) and the Fischer–Tropsch reactor (FT Reactor) through streams $\#H_2$ to RWGSR and #H2 to FT, respectively, following a molar distribution ratio of 1:2. The hydrogen distribution system operates at atmospheric pressure and 80 °C.

The H_2 stream (#H2 to RWGSR) and CO_2 stream ((#CO2) are first mixed in a mixer (Mix-100) at an H_2/CO_2 molar ratio of 1:1. The resulting mixture is subsequently compressed (K-100) and preheated (E-100) before being introduced into the RWGS reactor as the prepared feed stream operating at 750 °C and 2000 kPa.

Within the reactor, the RWGS reaction (Eq. 3) converts CO_2 into carbon monoxide (stream #CO), while water is produced as a by-product (stream #H2O ByProd.). The generated water is subsequently removed in a downstream separator (X-100), and the CO stream (stream #CO) is cooled using heat exchanger (E-101) before being directed to the FT reactor.

The CO stream (#CO to FT) reacts with the hydrogen stream ($\#H_2$ to FT) in the FT reactor after both streams are compressed (K-101) and preheated (E-102) to 350 °C and 2000 kPa. The reaction produces synthetic hydrocarbons, as represented in Eqs. (6)-(10).

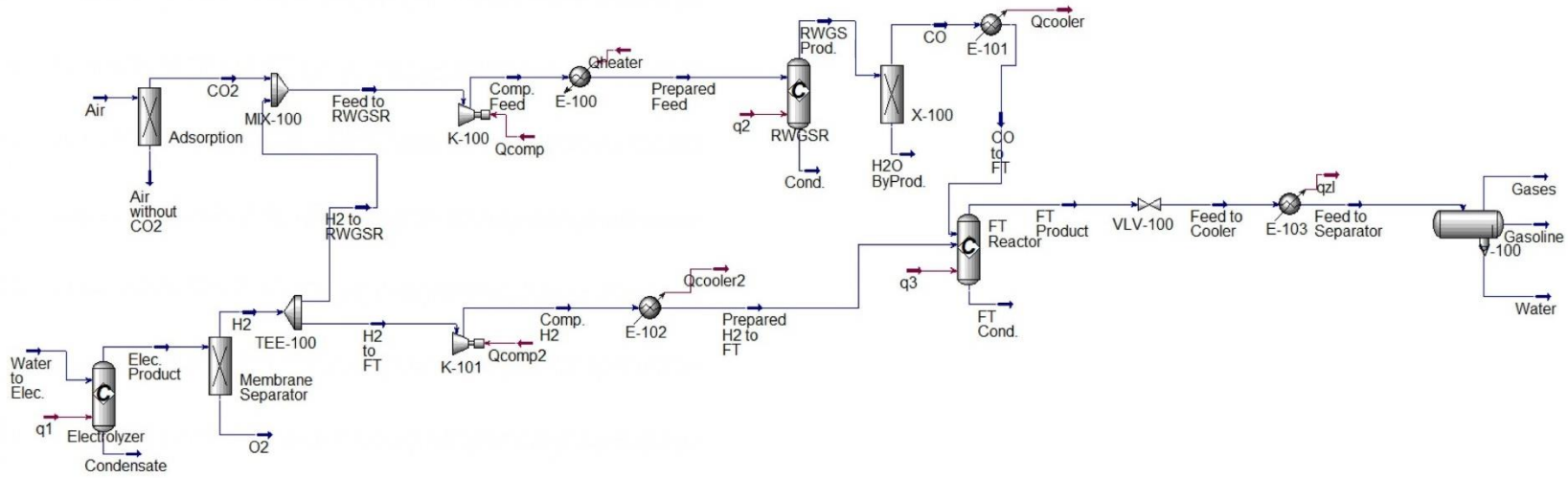

Figure 1. Plant design simulation developed using AspenOne Engineering® V14

Table 3. Mass flow rates, mass compositions, and operating conditions at the inlets and outlets of the EFPP units

Process	Inlet mass flow rate ($kg \cdot h^{-1}$) [a, b]	T (°C)	P (kPa)	Outlet mass flow rate ($kg \cdot h^{-1}$) [a, b]	T (°C)	P (kPa)
Absorption	#Air: $15{,}620 \times 10^3$ of Air (g)	50	101.3	#CO2: 9528 of CO_2 (g) # Air without CO2: $15{,}610 \times 10^3$ (g)	50	101.3
Electrolyzer	#Water to Elec.: 12,230 of H_2O (l)	25	101.3	#Elec. Product: 12,230 of H_2 (g)-O_2 (g) mix (with 88.81% O_2) #Condensate: 0 of H_2O (v)	80	101.3
Membrane Separator	#Elec. Product: 12,230 of H_2 (g)-O_2 (g) mix	80	101.3	#H2: 1368 of H_2 (g) #O2: 10,862 of O_2 (g)	80	101.3
Splitter: TEE-100	#H2: 1368 of H_2 (g)	80	101.3	#H2 to RWGSR: 437 of H_2 (g) #H2 to FT: 932 of H_2 (g)	80	101.3
Mixer: Mix-100	#CO2: 9528 of CO_2 (g)	50	101.3	#Feed to RWGSR: 9965 of H_2 (g)-CO_2 (g) mix	62.4	101.3
	#H2 to RWGSR: 437 of H_2 (g)	80				
Compressor: K-100	#Feed to RWGSR: 9965 of H_2 (g)-CO_2 (g) mix	62.4	101.3	#Comp. Feed: 9965 of H_2 (g)-CO_2 (g) mix	495	2000
Heater: E-100	#Comp. Feed: 9965 of H_2 (g)-CO_2 (g) mix	495	2000	#Prepared Feed: 9965 of H_2 (g)-CO_2 (g) mix	750	2000
RWGS Reactor: RWGSR	#Prepared Feed: 9965 of H_2 (g)-CO_2 (g) mix	750	2000	#RWGS Prod.: 9965 of CO (g)-H_2O (v) mix (with 60.86% CO)	750	2000
				#Cond. 0 of H_2O (l)		
Compressor: K-101	#H2 to FT: 932 of H_2 (g)	80	101.3	#Comp. H2: 932 of H_2 (g)	708	2000
Heat Exchanger: E-102	#Comp. H2: 932 of H_2 (g)	708	2000	#Prepared H2 to FT: 932 of H_2 (g)	350	2000
Separator: X-100	#RWGS Prod.: 9965 of CO (g)-H_2O (v) mix	750	2000	#CO: 6064 of CO (g)	751	2000
				#H2O ByProd.: 3900 of H_2O (g)		
Cooler: E-101	#CO: 6064 of CO (g)	751	2000	#CO to FT: 6064 of CO (g)	350	2000
FT Reactor: FT Reactor	#CO to FT: 6064 of CO (g)	350	2000	#FT Product: 6996 of a gaseous mixture, including e-fuels (g)	350	2000
	#Prepared H2 to FT: 932 of H_2 (g)			#FT Cond.: 0 of H_2O (l)		
Valve: VLV-100	#FT Product: 6996 of a gaseous mixture, including e-fuels (g)	350	2000	#Feed to Cooler: 6996 of a gaseous mixture, including e-fuels (g)	345	101.3
Cooler: E-103	#Feed to Cooler: 6996 of a gaseous mixture, including e-fuels (g)	345	101.3	#Feed to Separator: 6996 of a multiphase mixture, including e-fuels (g & l) (44.78 % vapour)	30	101.3
Three-phase separator: V-100	#Feed to Separator: 6996 of mixed gaseous products-e-fuels (g) mix	30	101.3	#Gases: 2298 of mixed gaseous products (g)	30	101.3
				#Gasoline: 1674 of e-fuels (l)		
				#Water: 3024 of H_2O (l)		

[a.] (g): gas; (v) : vapor; (l): liquid

[b.] #: Stream names in developed plant design using AspenOne Engineering® V14 (2022) (Fig. 1)

The resulting products consist of a gaseous mixture of hydrocarbons referred to as e-fuels. The primary e-fuel identified in this study is *n*-octane. The gaseous mixture is subsequently expanded through a valve (VLV-100) and cooled in a cooler (E-103) before being directed to a dedicated three-phase separator (V-100). In the final separation stage, the e-fuel is separated from the aqueous and gaseous phases under atmospheric pressure and a temperature of 30 °C.

The plant design requires auxiliary equipment, including heaters, coolers, heat exchangers, compressors, mixers, and control valves, to ensure proper operation and achieve the desired process conditions. These units maintain the specific temperature, pressure, and flow rate requirements necessary for the proper functioning of the reactors and other processing stages.

The integrated configuration offers several advantages compared with the various system designs reported in the existing literature (Farhani *et al.*, 2025; Pathak *et al.*, 2025; Bube *et al.*, 2024; Choi *et al.*, 2024; Farhani *et al.*, 2024; Pathak *et al.*, 2023; Wei *et al.*, 2017; Daza and Kuhn, 2016).

The system uses two environmentally sourced materials as its primary inputs, enabling the production of green hydrogen and sustainable synthetic fuels. The process contributes to reducing carbon emissions by converting atmospheric CO_2 into renewable synthetic fuels while its overall environmental performance largely depends on the renewable energy supplied to the integrated system.

4.2. Material balances

Table 3 provides a comprehensive overview of all major process units in the plant design, including the simulated inlet and outlet mass flow rates, as well as detailed information on stream composition, temperature, and pressure measurements.

The EFPP system relies on hydrogen production as a key component of the overall process. The electrolyzer coupled with the membrane separator produces 1,368 $kg \cdot h^{-1}$ of hydrogen (stream #H2 – see Figure 1) from 12,230 $kg \cdot h^{-1}$ of water (stream #Water to Elec.) according to Eq. (2). This hydrogen production rate is considered significant and is consistent with values reported in recent studies (Farhani *et al.*, 2025; Pathak *et al.*, 2025; Farhani *et al.*, 2024).

The produced hydrogen stream (#H2) is divided into two separate streams following the 1:2 molar ratio described in Section 3.1 (Plant Design). The first stream (437 $kg \cdot h^{-1}$) is directed to the Reverse Water–Gas Shift reactor (stream #H2 to RWGSR), where it reacts with 9528 $kg \cdot h^{-1}$ of CO_2 (stream #CO2) to produce 6064 $kg \cdot h^{-1}$ of CO (stream #CO). The required CO_2 is obtained through direct air capture from 15,620 × 10^3 $kg \cdot h^{-1}$ of atmospheric air (stream #Air). Although atmospheric air is abundantly available, direct air capture remains economically challenging, with reported costs ranging between 246 and 297 USD per ton of CO_2 (Dieterich *et al.*, 2020).

The second hydrogen stream (932 $kg \cdot h^{-1}$) is supplied to the Fischer–Tropsch reactor (stream #H_2 to FT). In the reactor, CO (stream #CO to FT: 6,064 $kg \cdot h^{-1}$) produced in the RWGS unit reacts with H_2 according to Eqs. (6)-(10), yielding 6996 $kg \cdot h^{-1}$ of a gaseous product mixture (stream #FT Product – Figure 1). This mixture consists of 17% CO, 2.17% H_2, 44.81% H_2O (vapor), 3.97% CH_4, 1.96% C_3H_8, and 30.09% *n*-octane.

The final products are separated in a three-phase separator (V-100) into 1674 $kg \cdot h^{-1}$ of 99.9% n-octane, representing the purified liquid synthetic hydrocarbon e-fuel (stream #Gasoline) and fulfilling the main objective of the study; 2298 $kg \cdot h^{-1}$ of a gaseous phase (stream #Gases) containing 51.75% CO; and 3024 $kg \cdot h^{-1}$ of an aqueous phase (stream #Water) (see Table 3).

The separated off-gas stream contains a significant amount of unconverted CO and is not intended for direct atmospheric discharge. Instead, the CO-rich stream can be collected and temporarily stored for subsequent utilization as a valuable intermediate feedstock in downstream processes. Carbon monoxide has potential applications in syngas-based operations, including fuel synthesis and chemical production, thereby providing an opportunity for additional resource recovery. This approach reduces carbon losses and enhances overall carbon utilization while offering flexibility in plant operation. Furthermore, utilizing the CO-containing stream as a recoverable product stream can improve the overall economic attractiveness and sustainability of the proposed process.

4.3. Energy balances

The main process units require thermal energy for heating and cooling operations, as presented in Table 4. Energy balances were performed for the Fischer–Tropsch reactor, electrolyzer, and CO_2 absorption unit to quantify their heat exchange rates with the surroundings. These calculations enabled the determination of actual utility requirements, which were subsequently used for the proper sizing of the auxiliary equipment and supporting systems.

Table 4. Energy-flow requirements of process units for heating and cooling

Process unit	Symbol[a]	Heat flow (MW)
Electrolyzer	q1	54.42
Compressor: K-100	Qcomp	1.93
Heater: E-100	Qheater	1.26
Compressor: K-101	Qcomp2	2.38
Heat Exchanger: E-102	Qcooler2	1.37
RWGS Reactor: RWGSR	q2	2.11
Cooler: E-101	Qcooler	0.77
FT Reactor: FT Reactor	q3	–8.27
Cooler: E-103	qzl	3.59

a. Heat flow names in developed plant design using AspenOne Engineering® V14 (2022) (Fig. 1)

The electrolyzer is the most energy-intensive component of the system, with an energy requirement of 54.42 MW, accounting for approximately 80% of total process energy demand of 67.84 MW. The electrolysis stage therefore represents the dominant energy-consuming process, which is consistent with findings reported in previous studies (Farhani *et al.*, 2025; Pathak *et al.*, 2025; Bube *et al.*, 2024; Choi *et al.*, 2024; Farhani *et al.*, 2024; Pathak *et al.*, 2023).

The system requires substantial renewable electricity for hydrogen production to qualify as green. Solar energy shows great potential for system development in this context. Saudi Arabia has a high solar capacity because its sunny climate allows global horizontal irradiance to reach 2000 to 2200 $kWh \cdot m^{-2} \cdot year^{-1}$ which positions it among the top countries in the world (Farhani *et al.*, 2025; Farhani *et al.*, 2024; Website 2). The high solar potential provides strong evidence for using large photovoltaic systems to meet electrolyzer requirements.

The energy balance calculations enabled the selection and sizing of the auxiliary equipment required to support reactor operations. The CO_2 stream from the absorption unit and the H_2 stream from the electrolyzer required both compression and thermal conditioning prior to entering the reactors. To achieve the required pressure and temperature conditions, the system incorporated two compressors (K-100 and K-101), one heater (E-100), one heat exchanger (E-102), and two coolers (E-101 and E-103).

The RWGS reactor requires a heating duty of 2.11 MW due to its endothermic nature, which necessitates continuous energy input. In contrast, the FT reactor operates as an exothermic system, releasing heat at a rate of −8.27 MW. The FT reactor therefore requires an effective heat removal system to ensure catalyst stability and maintain process safety. The product stream from the FT reactor is subsequently expanded through a valve system before entering the three-phase separator, where the final hydrocarbon products are recovered.

The plant thermal profile demonstrates that the electrical energy demand of electrolysis and the thermal management requirements of the FT heat removal system are interdependent. This highlights the importance of process integration and the implementation of energy optimization strategies.

4.4. Processes design and unit sizing

After completing the mass and energy balances and defining all stream operating conditions, mechanical design and equipment sizing of the most critical process units were carried out. This step ensures the technical feasibility of the proposed configuration and provides a link between process simulation and practical implementation.

Particular focus was placed on the Reverse Water Gas Shift reactor (RWGSR), Fischer–Tropsch reactor (FT Reactor), the heat exchanger (E-102), and the three-phase separator (V-100), given their strong influence on overall plant performance.

These units are presented as representative examples of the plant design methodology, demonstrating the translation of process-level calculations into industrially relevant equipment specifications.

4.4.1 Reverse water gas shift reactor and Fischer–Tropsch reactor

The RWGS and FT reactor sizing protocol followed established design standards requiring evaluation of operational performance.

The RWGS reactor is a vertical vessel supported on concrete pads, with a total capacity of 71.16 m^3, a diameter of 3.10 m, and a height of 9.30 m. The system is equipped with a propeller agitator operating at 420 rpm, resulting in an agitation power requirement of 142.32 kW (Table 5).

The FT reactor has a total volumeof 723.24 m^3, a diameter of 6.75 m, and a height of 20.25 m. It operates with the same propeller system at 420 rpm but requires 1446.48 kW power to operate (Table 5).

Both reactors are constructed from carbon steel, with vessel wall thicknesses of 40 mm for the RWGS reactor and 68 mm for the FT reactor. They are equipped with ellipsoidal heads and closures. In addition, the reactors are fitted with jackets maintaining a 150 mm spacing to ensure effective temperature control.

The RWGS reactor is insulated with asbestos–diatomaceous earth insulation with a thickness of 32 mm, while the FT reactor uses 85% magnesia insulation with the same thickness.

These design choices ensure the required mechanical strength, adequate mixing performance, and effective thermal transfer efficiency, thereby meeting the operational requirements of the reactors.

Table 5. Reverse water gas shift and Fischer–Tropsch reactors specifications.

Reactor	**RWGS reactor**	**FT reactor**
Configuration and support	Vertical vessel on concrete pads	Vertical vessel on concrete pads
Volume (m^3)	71.16	723.24
Diameter (m)	3.10	6.75
Height (m)	9.30	20.25
Impeller type	Propeller 420 rpm	Propeller 420 rpm
Agitation power (kW)	142.32	1446.48
Material of construction	Carbon steel	Carbon steel
Vessel thickness (mm)	40	68
Head and closure	Ellipsoide	Ellipsoide
Thermal insulation type	Asbestos-diatomaceous earth mixture	85% magnesia
Thermal insulation thickness (mm)	32	32
Jacket spacing (mm)	150	150

4.4.2 Heat exchanger

The design specifications for heat exchanger E-102 are presented in Table 6.

This shell-and-tube exchanger operates at a thermal capacity of 1.37 MW (see Table 4). The unit follows TEMA AEL standards through the use of a fixed tubesheet design. The heat exchanger consists of 128 tubes arranged in a square pitch configuration, with one shell pass and one tube pass, enabling efficient heat transfer through optimized flow conditions.

The tube pitch is 20 mm, while the tube bundle diameter is 0.29 m and the shell diameter is 0.3 m. Each tube has an outer diameter of 16 mm, a wall thickness of 3.2 mm and an inner diameter of 9.6 mm, with a length of 1.83 m, resulting in a total heat transfer area of 11.712 m^2. The heat exchanger is equipped with baffles spaced at 0.12 m with a 25% baffle cut to enhance fluid distribution and reduce shell-side pressure drop.

Table 6. Heat exchanger E-102 design details

Q (MW)	1.37
Shell Passe	1
Tube Passe	1
Type	Fixed and U-tube
A (m^2)	11.71
No. tubes	128
Tube arrangement	square
Tube pitch (mm)	20
Bundle diameter (m)	0.29
Shell diameter (m)	0.3
Baffle spacing (m)	0.12
Baffle cut (%)	25
Tube Dimensions	
d_o (mm)	16
t (mm)	3.2
d_i (mm)	9.6
L (m)	1.83

4.4.3 Three-phase separator

The three-phase separator V-100 is a horizontal, saddle-mounted vessel equipped with a demister pad to ensure efficient gas–liquid separation (Table 7).

Table 7. Three-phase separator design details

Configuration and support	Horizontal tank on concrete saddle support with demister pad
Diameter (m)	1.1
Length (m)	3.3
Weir height (m)	0.55
Material of construction	Carbon steel
Vessel thickness (mm)	5
Head and closure	Torispherical

The device has a diameter of 1.1 m and a length of 3.3 m, providing sufficient volume for the separation of gas, hydrocarbon oil, and aqueous phases. A stable liquid level is maintained by a weir height of 0.55 m. The vessel is constructed from carbon steel with a wall thickness of 5 mm, enabling it to withstand operational pressure. Its torispherical heads provide both pressure resistance and compactness, which are key advantages for industrial-scale separation.

Industrial processes require safe and efficient operation through precise reactor, heat exchanger, and three-phase separator design. The units are essential components that enable chemical reactions to proceed effectively while ensuring proper heat transfer and efficient phase separation oil and gas production systems.

4.5. Economic results

The economic assessment of the proposed e-fuel production plant (EFPP) was performed using the methodology presented in Section 3. Particular attention was given to the influence of electricity demand because hydrogen generation through water electrolysis represents the dominant energy consumer within the system.

The total power demand of the process was estimated as 67.84 MW, of which the electrolyzer accounted for 54.42 MW, representing approximately 80% of the total energy requirement. Using Eq. (30), the annual operating time was estimated to be $t_{op} = 7884\ h \cdot year^{-1}$. The annual electricity consumption of the electrolyzer was therefore estimated to be $E_{annual} = 54{,}420 \cdot 7884 = 4.29 \cdot 10^{8}\ kWh \cdot year^{-1}$. Using the Saudi industrial electricity price of 0.048 USD·kWh^{-1}, the annual electrolysis cost was estimated as $C_{elec} = 20.59\ million\ USD \cdot year^{-1}$.

The DAC process represents another significant economic contributor because of the large quantity of CO_2 required for fuel production. Based on the process mass balance, 9528 kg·h^{-1} of CO_2 is captured and supplied to the system. The annual captured CO_2 amount becomes $\dot{m}_{CO_2} = 9528 \cdot 7884 = 7.51 \cdot 10^{7}\ kg \cdot year^{-1}$. Using the reported DAC cost range of 246–297 USD/t_{CO2}, the annual DAC cost was estimated as: $C_{DAC} = 18.47 - 22.30\ million\ USD \cdot year^{-1}$.

The e-fuel production rate obtained from the process simulation was 1674 kg·h^{-1} of n-octane. Using density value of 706 kg·m^{-3} (obtained from AspenOne Engineering® results), the annual fuel production was estimated as $1674 \cdot 7884 / 706 = 1.87 \cdot 10^{4}\ m^{3} \cdot year^{-1}$, corresponding to approximately 18.7 million liters per year.

The sensitivity analysis showed that electricity price exerts the strongest influence on the process economics. Increasing electricity prices by 30% significantly increases the annual operating cost because of the high electricity requirement of hydrogen production. Variations in DAC cost and plant capacity factor also affected the overall economics but to a lower extent.

The results indicate that electricity consumption and CO_2 capture costs constitute the major economic limitations of the proposed process. Therefore, reductions in renewable electricity costs and improvements in DAC technology are expected to significantly improve the economic competitiveness of synthetic e-fuel production. Similar trends have been reported in previous Power-to-Liquid studies (Dieterich *et al.*, 2020; Bube *et al.*, 2024; Chauvy and Dubois, 2022b).

To investigate the influence of renewable energy integration, an additional scenario was evaluated assuming that the total electricity demand of the process is supplied entirely by renewable energy sources. In this case, the Levelized Cost of Electricity (LCOE) of renewable systems was used instead of industrial grid electricity prices. Typical values reported for large-scale renewable projects in Saudi Arabia range between 0.02 and 0.03 USD/kWh for solar photovoltaic systems, with a representative value of 0.025 USD/kWh adopted in this study (IEA, 2023; IRENA, 2024). Under this renewable-energy scenario, the annual electrolysis cost decreased from 20.59 million USD/year to approximately 10.72 million USD/year, corresponding to a reduction of nearly 48%. The electricity-related production cost of e-fuel was estimated at 0.57 USD/L. When direct air capture (DAC) costs were also included, the total production cost increased to 1.55–1.76 USD/L. These results highlight that while renewable electricity integration significantly improves the economic performance of the proposed e-fuel production system, CO_2 capture remains a dominant cost factor in the overall process pathway (Dieterich *et al.*, 2020; IRENA, 2024).

5. CONCLUSION

The study investigated synthetic e-fuels as a sustainable alternative to conventional fossil fuels, offering an environmentally friendly pathway for fuel production. The process integrates renewable energy to produce hydrogen *via* water electrolysis and captures carbon dioxide through direct air capture (DAC), enabling the conversion of atmospheric CO_2 into valuable hydrocarbon products. Overall, the system provides an effective route for reducing greenhouse gas emissions by utilizing renewable electricity, water, and air as primary feedstocks.

Material and energy balances were established based on a reference demand corresponding to the fuel consumption of approximately 10,000 individuals, equivalent to 1674 $kg \cdot h^{-1}$ of n-octane production. The system requires 1368 $kg \cdot h^{-1}$ of H_2 and 9528 $kg \cdot h^{-1}$ of CO_2, which are produced from 12,230 $kg \cdot h^{-1}$ of water and 15,620 $\times$ 10^3 $kg \cdot h^{-1}$ of atmospheric air, respectively. These results indicate that decentralized e-fuel production is associated with significant resource demands.

The electrolyzer is the most energy-intensive unit in the process, requiring 54.42 MW of power, while the RWGS reactor and heat exchangers consume 2.11 MW and approximately 1.37 MW, respectively. These findings confirm that hydrogen production dominates the overall energy demand and is the key factor influencing system sustainability.

From an economic perspective, the total electricity demand of the process was estimated at 67.84 MW, with the electrolyzer accounting for approximately 80% of the total energy consumption. Under a renewable electricity scenario (LCOE = 0.025 USD/kWh), the annual electrolysis cost was reduced by nearly 48%, from 20.59 million USD/year to 10.72 million USD/year. Consequently, the e-fuel production cost was estimated at 1.55–1.76 $USD \cdot L^{-1}$, highlighting the strong dependence of process economics on electricity price and CO_2 capture costs.

The main process units—including the RWGS reactor, Fischer–Tropsch reactor, heat exchanger, and three-phase separator—were designed, sized, and fully specified, demonstrating the technical feasibility of the integrated configuration.

Overall, the proposed system represents a technically viable pathway for sustainable fuel production with significant potential environmental benefits. Future work should focus on advanced process integration, optimization of renewable energy utilization, and further economic improvement strategies to enhance system efficiency and industrial feasibility.

Supplementary Data

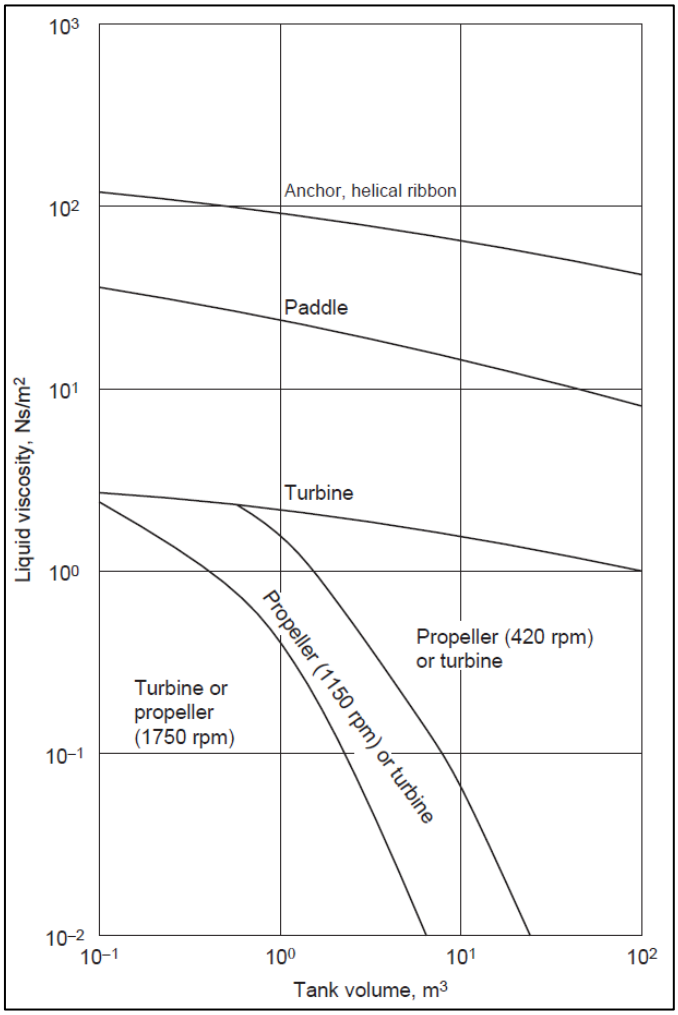

Figure S1. Agitator selection guide (Towler and Sinnott, 2008).

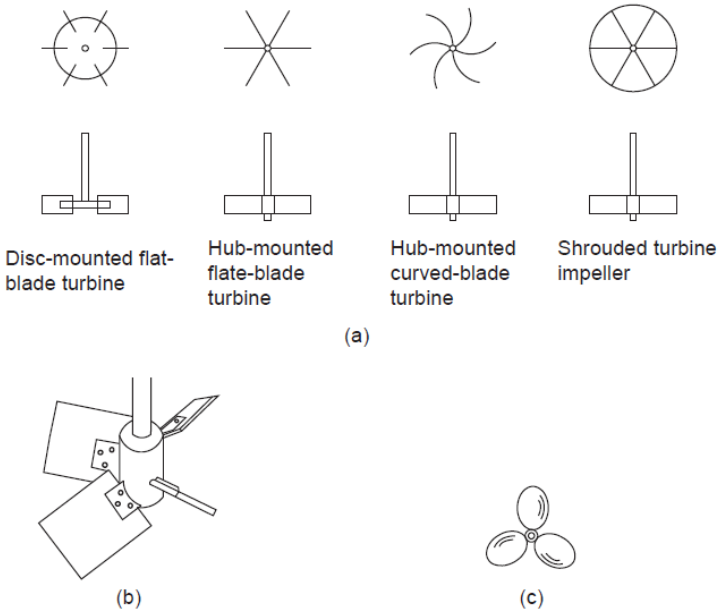

Figure S2. Basic impeller types. (a) Turbine impeller. (b) Pitched-bladed turbine. (c) Marine propeller (Towler and Sinnott, 2008).

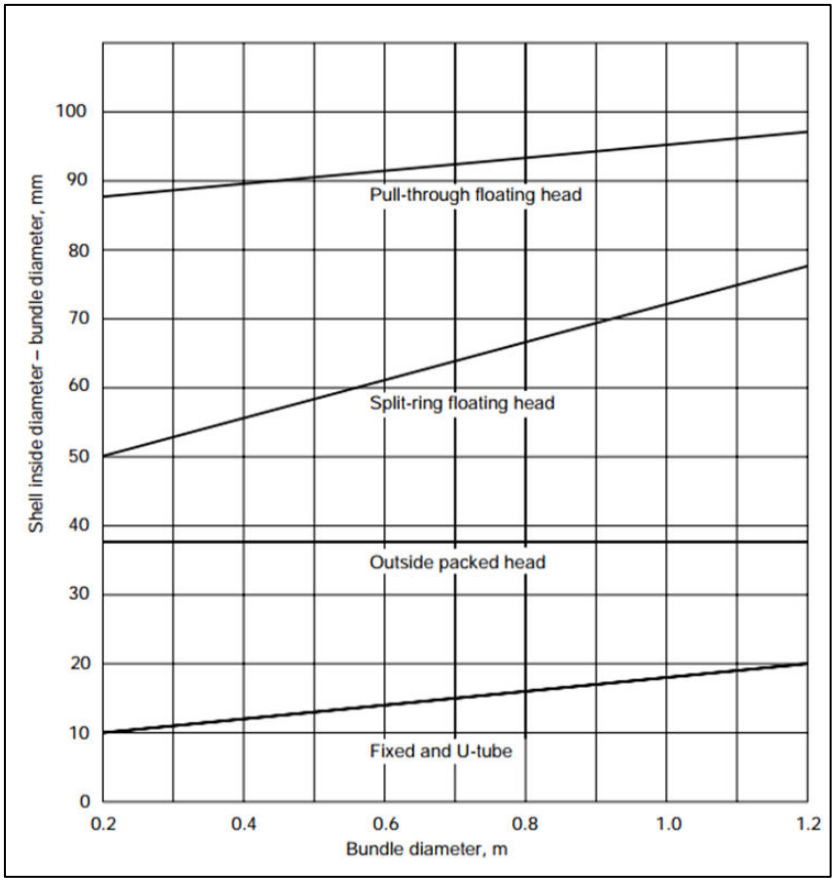

Figure S3. Shell-to-bundle diametral clearance (Towler and Sinnott, 2008).

Table S1. Power requirements for baffled agitated tanks (Towler and Sinnott, 2008).

Agitation	Applications	Power (kW/m^3)
Mild	Blending, mixing	0.04–0.10
	Homogeneous reactions	0.01–0.03
Medium	Heat transfer	0.03–1.0
	Liquid–liquid mixing	1.0–1.5
Severe	Slurry suspension	1.5–2.0
	Gas absorption	1.5–2.0
	Emulsions	1.5–2.0
Violent	Fine slurry suspension	> 2.0

Table S2. Heuristics for vessels (pressure and storage) (Turton *et al.*, 2012)

Pressure Vessels					
1. Design temperature between −30 °C and 345 °C is 25 °C above the maximum operating temperature; higher safety margins are used outside the given temperature range. 2. The design pressure is 10% or 0.69–1.7 bar (10–25 psi) over the maximum operating pressure, whichever is greater. The maximum operating pressure, in turn, is taken as 1.7 bar (25 psi) above the normal operation. 3. Design pressures of vessels operating at 0–0.69 bar (0–10 psig) and 95–540 °C (200–1000 °F) are 2.76 barg (40 psig). 4. For vacuum operation, design pressures are 1 barg (15 psig) and full vacuum. 5. Minimum wall thickness for rigidity: 6.4 mm (0.25 in) for 1.07 m (42 in) diameter and less than 8.1 mm (0.32 in) for 1.07–1.52 m (42–60 in) diameter, 11.7 mm (0.38 in) for more than 1.52 m (60 in) diameter. 6. Corrosion allowance 8.9 mm (0.35 in) for known corrosive conditions, 3.8 mm (0.15 in) for non-corrosive streams, and 1.5 mm (0.06 in) for steam drums and air receivers. 7. Allowable working stresses are one-fourth of the ultimate strength of the material. 8. Maximum allowable stress depends sharply on temperature.					
Temperature: (°F)		−20 to 650	750	850	1000
(°C)		(−30 to 345)	400	455	540
Low alloy steel SA-203	(psi)	18,759	15,650	9,950	2,500
	(bar)	1290	1070	686	273
Type 302 stainless steel	(psi)	18,750	18,750	15,950	6,250
	(bar)	1290	1290	1100	431

Table S3. The constants K_1 and n_1 for bundle diameter equation (Towler and Sinnott, 2008)

Triangular pitch, $p_t = 1.25 \times d_o$					
No. of passes	**1**	**2**	**4**	**6**	**8**
Triangular pitch, $p_t = 1.25 \times d_o$					
K_1	0.319	0.249	0.175	0.0743	0.0365
n_1	2.142	2.207	2.285	2.499	2.675
Square pitch, $p_t = 1.25 \times d_o$					
K_1	0.215	0.156	0.158	0.0402	0.0331
n_1	2.207	2.291	2.263	2.617	2.643

References

Alwosheel, A., Dua, R., 2023, Estimating Regional Variation In Saudi Arabia's Energy Usage And Carbon Emissions. King Abdullah Petroleum Studies and Research Center (KAPSARC). Available at: https://www.kapsarc.org/research/publications/estimating-regional-variation-in-saudi-arabias-energy-usage-and-carbon-emissions/.

Aspen Technology, Inc., AspenOne Engineering® Version 14, Aspen Technology, Inc., 2022. Available at: https://www.aspentech.com.

Bube, S., Bullerdiek, N., Voß, S., Kaltschmitt, M., 2024. Kerosene Production from Power-Based Syngas – A Technical Comparison of The Fischer-Tropsch and Methanol Pathway, Fuel 366, no. 131269.

Chauvy, R., Dubois, L., 2022a. Life Cycle And Techno-Economic Assessments of Direct Aircapture Processes: An Integrated Review, International Journal of Energy Research 46, p. 10320–10344.

Chauvy, R., Dubois, L., 2022b. Techno-Economic Analysis of CO_2 Direct Air Capture Processes, Energy Conversion and Management 260, no. 115615.

Choi, Y., Sim, G. D., Jung, U., Park, Y., Youn, M. H., Chun, D. H. , Rhim, G. B., Kim, K. Y., Koo, K. Y., 2024. Copper Catalysts for CO_2 Hydrogenation to CO Through Reverse Water–Gas Shift Reaction for E-Fuel Production: Fundamentals, Recent Advances, and Prospects, Chemical Engineering Journal 492, no. 152283.

Daza, Y. A., Kuhn, J. N., 2016. CO_2 Conversion by Reverse Water Gas Shift Catalysis: Comparison of Catalysts, Mechanisms and Their Consequences For CO_2 Conversion to Liquid Fuels, RSC Advances 6, p. 49675-49691.

Dieterich, V., Buttler, A., Hanel, A., Spliethoff, H., Fendt, S., 2020. Power-to-Liquid *Via* Synthesis of Methanol, DME or Fischer–Tropsch-Fuels: A Review, Energy & Environmental Science 13(10), p. 3207-3252.

Fang, Z., Smith, Jr. R. L., Qi, X., 2015. Production of Hydrogen from Renewable Resources. Springer, Dordrecht.

Farhani, S., Alharbi, S. S., Alharbi, S. S., Barhoumi, E. M., Bacha, F., 2025. Investigation and Analysis of Solar and Wind Energy Potential for Green Hydrogen Production *via* Alkaline Water Electrolysis, IEEE Access 13, p. 168878.

Farhani, S., Barhoumi, E. M., Ul Islam, Q., Bacha, F., 2024. Optimal Design and Economic Analysis of A Stand-Alone Integrated Solar Hydrogen Water Desalination System Case Study Agriculture Farm In Kairouan Tunisia, International Journal of Hydrogen Energy 63, p. 759.

Fox, J.M., Degen, B.D.,Cady, Grover, Deslate, F.D., Summers, R.L. 1991. Slurry Reactor Design Studies: Slurry vs. Fixed-Bed Reactors for Fischer–Tropsch and Methanol: Final Report. U.S. Department of Energy.

González-Castaño, M., Dorneanu, B., Arellano-García, H., 2021. The Reverse Water Gas Shift Reaction: A Process Systems Engineering Perspective, Reaction Chemistry & Engineering 6, p. 954-976.

Hassan, D. M., Gosselin, R., Abatzoglou, N., 2025. Modelling Fischer–Tropsch Synthesis: A Review of Applications Using Genetic Algorithms and Hybrid GA–Based Models, Chemical Engineering Journal Advances 24, no. 100958.

Intergovernmental Panel on Climate Change (IPCC), 2022. "Climate Change 2022–Mitigation of Climate Change. Working Group III Contribution to the Sixth Assessment Report of the Intergovernmental Panel on Climate Change, v. 2 : pbk" Priyadarshi R. Shukla *et al.*, *et al.*, Editor, Cambridge, Cambridge University Press, 2022, ISBN: 9781009423915 (v. 2 : pbk).

Intergovernmental Panel on Climate Change (IPCC), 2023. "Climate Change 2021–The Physical Science Basis: Working Group I Contribution to the Sixth Assessment Report of the Intergovernmental Panel on Climate Change," Valérie Masson-Delmotte*et al.*, Editor, Cambridge, Cambridge University Press, 2023, ISBN : 9781009157896 ebook.

International Energy Agency (IEA), 2023. Renewables 2023: Analysis and forecast to 2028. IEA, Paris. Available at: https://www.iea.org/reports/renewables-2023

International Renewable Energy Agency (IRENA), 2024. Renewable Power Generation Costs in 2023. IRENA, Abu Dhabi. Available at: https://www.irena.org/Publications/2024/Jul/Renewable-Power-Generation-Costs-in-2023

Ivanov, Y., Pyatnichko, O., Zhuk, H., Onopa, L., Soltanibereshne, M., 2017. Extraction of Carbon Dioxide from Gas Mixtures with Amines Absorbing Process, Energy Procedia 128, p. 240–247.

Keith, D. W., Holmes, G., Angelo, D. St., Heidel, K., 2018. A Process for Capturing CO_2 From the Atmosphere, Joule 2(8), p. 1573-1594.

Kierzkowska-Pawlak, H., Chacuk, A. 2010. Kinetics of Carbon Dioxide Absorption Into Aqueous MDEA Solutions, Ecological Chemistry and Engineering, S 17, p. 463-475.

Li , W., Lin, Q., Lv, Y., Li, H., Liu, W., Liu, Y., Zhang, M., Men, Z. 2025. Optimization Strategy And Research Progress Of Ironbased Fischer–Tropsch Synthesis Catalysts: A Green And Low-Carbon Perspective. Clean Energy 9(5), p. 39–54.

Masuku, C. M., Shafer, W, D., Ma, W., Gnanamani, M. K., Jacobs, G., Hildebrandt, D., Glasser, D., Davis, B. H., 2012. Variation Of Residence Time With Chain Length For Products In A Slurry-Phase Fischer–Tropsch Reactor. Journal of Catalysis 287, p. 93–101.

Pathak, P. K., Yadav, A. K., Kamwa, I., 2025. Green Hydrogen: A Strategic Energy Vector for Achieving Net-Zero Emissions by 2050, Sustainable Energy & Fuels 9, p. 5218.

Pathak, P. K., Yadav, A. K., Padmanaban, S., 2023. Transition Toward Emission-Free Energy Systems by 2050: Potential Role of Hydrogen, International Journal of Hydrogen Energy 48(26), p. 9921.

Peters, M. S., Timmerhaus, K. D., West, R. E., 2003. Plant Design and Economics for Chemical Engineers, fifth edition, McGraw-Hill Companies, Inc., New York.

Phey, M., Abdullah, T., Ali, U., Mohamed , M., Ikram, M., Nabgan , W., 2023. Reverse Water Gas Shift Reaction Over A Cu/Zno Catalyst Supported on Regenerated Spent Bleaching Earth (RSBE) in A Slurry Reactor: The Effect of The Cu/Zn Ratio on The Catalytic Activity. RSC Advances 13, no. 3039.

Santos, S., Gomes, J., Bordado, J., 2014. Comparative Study of Amine Solutions Used in Absorption/Desorption Cycles of CO_2, LAP LAMBERT Academic Publishing, Saarbrücken.

Sanz-Pérez, E. S., Murdock, C. R., Didas, S. A., Jones, C. W., 2016. Direct Capture of CO_2 from Ambient Air, Chemical Reviews 116(19), p. 11840–11876.

Saudi Electricity Regulatory Authority (SERA), 2026. Consumption Tariff. Available at: SERA Consumption Tariff Page: https://www.sera.gov.sa/en/consumer/electric-tariff/electric-tariff-categories/consumption-tariff (Accessed on June 21, 2026).

Sinnott, R. K., 2005. Chemical Engineering Design, fourth edition, Elsevier Butterworth-Heinemann, Oxford.

Torres-Sempere, G., González-Arias, J., Penkova, A., Santos-Muñoz, J. L., Bobadilla, L. F., Odriozola, J. A., Pastor-Pérez L., Reina T. R., 2025. CO_2 Conversion *via* Low-Temperature RWGS Enabled by Multicomponent Catalysts: Could Transition Metals Outperform Pt?, Topics in Catalysis 68, p. 114–125.

Towler, G., Sinnott, R., 2008, Chemical engineering Design - Principles, practice and Economics of plant and Process design, Elsevier Inc., third edition, Butterworth-Heinemann, United States of America.

Turton, R., Bailie, R. C., Whiting, W. B., Shaeiwitz, J. A., Bhattacharyya, D., 2012. Analysis, Synthesis, and Design of Chemical Processes, fourth edition, Pearson Education, Inc., New Jersey.

Versteeg, G.F., Swaaij, W.P.M. van, 1988. On the Kinetics Between CO_2 and Alkanolamines Both in Aqueous and Non-aqueous Solutions—I. Primary and Secondary Amines, Chemical Engineering Science 43(3), p. 573-585.

Wei, J., Ge, Q., Yao, R., Wen, Z., Fang, C., Guo, L., Xu, H., Sun, J., 2017. Directly Converting CO_2 Into A Gasoline Fuel, Nature Communications 8, no. 15174.

Yu, C. H., Huang, C. H., Tan, C. S., 2012. A Review of CO_2 Capture by Absorption and Adsorption, Aerosol and Air Quality Research 12(5), p. 745–769.

Website 1: https://ycharts.com/indicators/saudi_arabia_oil_consumption_tonnes (Accessed on May 10, 2025).

Website 2: https://www.stats.gov.sa/ar/statistics-tabs?tab=436312&category=124797 (Accessed on October 4, 2025).